

Ball and Plate System Controller Using State Observer and Geometric Approach

Khalid Lefrouni^{1,*}, Saoudi Taibi²

^{1,2}Department of Mechanical Engineering, Mohammed V University in Rabat, Rabat, Morocco

(Received: January 15, 2025; Revised: February 20, 2025; Accepted: May 25, 2025; Available online: July 19, 2025)

Abstract

The primary objective of this paper is to present a feedback regulator using a Luenberger observer for state estimation of the ball-plate system, which is characterized by high instability and non-linearity. The novelty of this work lies in the design of an innovative control approach that explicitly considers time delay in the feedback loop—an aspect often neglected in prior studies. The adopted methodology involves modeling the system in state space while accounting for delay, and then constructing a state-feedback observer using a geometric approach. Numerical simulations were conducted to validate the proposed design. For instance, with an observer gain of $L_2 = [1.58, 1.35]$, the controller minimizes response time along the x-axis and remains stable for delays up to 0.6364 seconds. Similarly, along the y-axis, a gain of $L_5 = [0.58, 0.27]$ ensures robustness even with delays up to 1.4084 seconds, while effectively reducing initial overshoot. In all tested scenarios, estimation errors converged to zero, confirming the effectiveness of the observer-based controller. These findings support future work on automatic gain tuning based on performance specifications.

Keywords: Ball And Plate System, Delay Systems, State-Feedback Observer, Geometric Approach, Frequency Analysis, Luenberger Observer

1. Introduction

The ball and plate system [1], similar to the levitation-magnetic system [2] and the ball and beam system [3], [4], exhibits intricate dynamics as a result of its inherent instability and nonlinearity. Consequently, it has garnered significant attention in the fields of engineering education and research. The primary benefits of this system include its ease of implementation and the opportunity it provides for experimentally validating theoretical concepts in areas such as control, analysis, and other engineering fields [5], [6].

A multitude of works are documented in the literature. The ball-plate mechanism in [7], [8] utilizes electromagnetic actuators to achieve 2 degrees of motion. A control law is designed for this system to adjust the ball's position based on a Lyapunov-based approach. The Linear Quadratic Regulator (LQR) is introduced in [9], [10]. The authors in [11], [12] examine the utilization of a PD position controller for regulating the system. A novel variant of controller, known as dual PD controller, is introduced in [13] to control the ball's position. The literature [14], [15] examines and contrasts two control strategies: the PID and a controller based on the sliding mode. Four controllers are compared in [16], PID controller, sliding mode controller, linear-quadratic regulator, and fuzzy controller.

Nonetheless, these investigations were typically conducted using simplified system models [17], [18], [19] that neglected the delay inherent in the control loop. This paper proposes the integration of an observer [20] to evaluate the system state while considering feedback latency. To accomplish this objective, a state feedback control law [21] will be employed in conjunction with a frequency-domain method known as the geometric approach [1], [22].

The subsequent sections of this article are structured as follows. Section 2 introduces a system modeling approach that considers the influence of feedback latency. In Section 3, a Luenberger observer [23] is constructed to accurately predict the system's state. In Section 4, the accuracy of the outcomes derived from the simulation is validated. To conclude, Section 5 presents our results and outlines our plans for future work.

*Corresponding author: Khalid Lefrouni (lefrouni@emi.ac.ma)

DOI: <https://doi.org/10.47738/jads.v6i3.783>

This is an open access article under the CC-BY license (<https://creativecommons.org/licenses/by/4.0/>).

© Authors retain all copyrights

2. Ball - Plate System Modelling

Using Lagrange's method, we developed a mathematical representation of the system (figure 1), which forms the basis for the control law designed in this article. The subsequent section provides a detailed explanation of the methodology employed. Lagrange's technique allows us to determine the model that describes the system's dynamics through the subsequent equations:

$$\frac{\partial}{\partial t} \left(\frac{\partial L}{\partial \dot{x}} \right) - \frac{\partial L}{\partial x} = 0 \tag{1}$$

$$L = E_k - E_p \tag{2}$$

E_k is the kinetic energy and E_p is the potential energy.

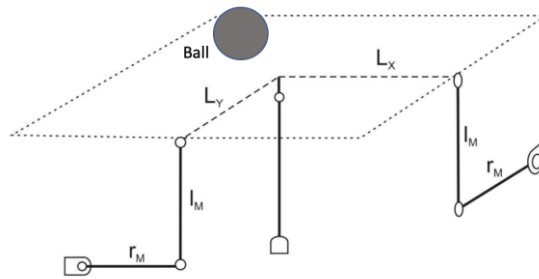


Figure 1. Structure of the ball and plate system

To simplify the initial dynamic modeling, we begin by disregarding slippage between the ball and the plate. The assumption of disregarding slippage, as stated, is made primarily to simplify the initial model derivation and focus on the core control and observation problem. While this is a common simplification in foundational studies of ball-and-plate systems (figure 2), we acknowledge its potential influence on real-world applicability. In practice, especially during rapid plate accelerations or if the ball/plate surfaces have low friction coefficients, slippage can occur. This unmodeled dynamic could lead to a mismatch between the predicted and actual ball position, potentially degrading the controller's tracking performance and, in extreme cases, affecting its robustness. Future extensions of this work could incorporate slip models or adaptive/robust control techniques to mitigate these effects and enhance performance across a wider range of operating conditions.

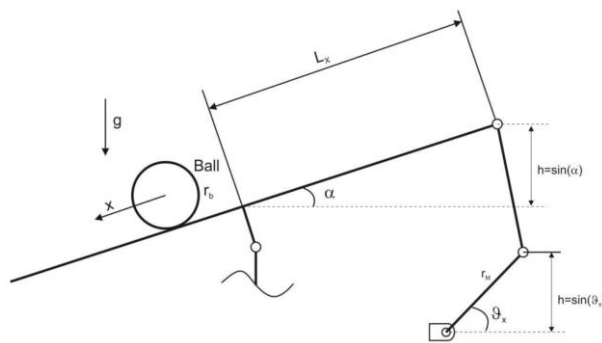


Figure 2. View of the ball and plate system from the side

Under this assumption, the expressions for E_k and E_p can then be formulated as:

$$E_k = \frac{1}{2} m_b (\dot{x}_b^2 + \dot{y}_b^2) + \frac{1}{2} J_b \omega_b^2 \tag{3}$$

$$E_p = -m_b g x_b \sin(\alpha) - m_b g y_b \sin(\beta) \tag{4}$$

By applying (1), where the Lagrangian L is defined in (2), we obtain:

$$\frac{\partial}{\partial t} \left(\frac{\partial L}{\partial \dot{x}} \right) = \frac{\partial}{\partial t} \left(\left(m_b + \frac{J_b}{r_b^2} \right) \dot{x}_b \right) = \left(m_b + \frac{J_b}{r_b^2} \right) \ddot{x}_b \quad (5)$$

and

$$\frac{\partial L}{\partial x} = m_b g \sin(\alpha) \quad (6)$$

Thus, by substituting equations (5) and (6) into (1), we obtain (7), which describes the ball's motion along the x-axis.

$$\ddot{x}_b = \frac{m_b g r_b^2}{m_b r_b^2 + J_b} \sin(\alpha) \quad (7)$$

Equation (7) describes the ball's trajectory in the x direction. In this case, the controller controls the angle ϑ_x , and this is accomplished by employing the subsequent formula:

$$\sin(\vartheta_x) r_M = \sin(\alpha) L_X = h \quad (8)$$

Thus, the equation relating the input ϑ_x and the output x_b is determined :

$$\ddot{x}_b = \frac{m_b g r_b^2 r_M}{(m_b r_b^2 + J_b) L_X} \sin(\vartheta_x) \quad (9)$$

In the same way, by applying this method, the equation representing the ball's motion on the y-axis is:

$$\ddot{y}_b = \frac{m_b g r_b^2 r_M}{(m_b r_b^2 + J_b) L_Y} \sin(\vartheta_y) \quad (10)$$

Further simplification of the model is achieved by assuming minimal fluctuation of ϑ_x and ϑ_y .

The simplification assuming minimal fluctuation of the plate angles ϑ_x and ϑ_y (i.e., $\sin(\vartheta_x) \approx \vartheta_x$) is employed to linearize the system model. This linearization is standard practice as it significantly facilitates the design and analysis of linear control strategies, such as the state-feedback controller and Luenberger observer used in this study. While this approximation is generally valid for small deviations around the plate's horizontal equilibrium – a common operational regime for such control tasks – we recognize that for larger angular movements, the non-linear $\sin(\vartheta_x)$ term would become more significant. This could lead to a discrepancy between the simplified model and the actual system dynamics, potentially affecting the controller's performance precision and stability margins when operating far from the equilibrium where the approximation is less accurate. A formal sensitivity analysis or the application of non-linear control techniques could be explored in future work to quantify these effects or extend the operating range.

With this assumption, where $\sin(\vartheta_x) \approx \vartheta_x$ and $\sin(\vartheta_y) \approx \vartheta_y$ (small angle approximation), the ball's movement, previously described by (9) and (10), can be further simplified to:

$$\ddot{x}_b = G_x \vartheta_x \quad (11)$$

$$\ddot{y}_b = G_y \vartheta_y \quad (12)$$

With $G_x = \frac{m_b g r_b^2 r_M}{(m_b r_b^2 + J_b) L_X}$ and $G_y = \frac{m_b g r_b^2 r_M}{(m_b r_b^2 + J_b) L_Y}$

Note: Due to the similarities of the models for both axes, we will focus on studying the control law specifically for the x-axis. We will then derive the conclusions for the y-axis.

Considering the feedback latency τ_{1x} , the state-space model of the system in the x-direction is given by:

$$\begin{cases} \dot{x}(t) = A x(t) + B u(t - \tau_{1x}) \\ y(t) = C x(t) \end{cases} \quad (13)$$

The state vector $x(t)$ represents the ball's position and velocity along the x-axis, the input $u(t)$ is the plate's tilt angle, and the output $y(t)$ is the ball's position. Specifically, these are defined as:

State vector: $x(t) = [x_b(t) \quad \dot{x}_b(t)]^T$

Input: $u(t) = \vartheta_x(t)$

Output: $y(t) = x_b(t)$

From the simplified dynamics (9) for the x-direction, $\ddot{x}_b = G_x \vartheta_x(t)$, we can derive the state-space matrices as follows: Let $x_1 = x_b$ and $x_2 = \dot{x}_b$.

Then $\dot{x}_1 = x_2$ and $\dot{x}_2 = \ddot{x}_b = G_x u(t)$.

This leads to the matrices:

$$A = \begin{bmatrix} 0 & 1 \\ 0 & 0 \end{bmatrix}, \quad B = \begin{bmatrix} 0 \\ G_x \end{bmatrix}, \quad C = [1 \quad 0]$$

3. State-Feedback Controller with Observer

3.1. The Luenberger Observer

The primary aim of this study is to establish an observer for monitoring the state of the system, based on the principles of the Luenberger observer [23]. This type of observer is central to model-based control and estimation theory [24]. Model (12) defines the observer configuration employed, allowing the convergence of the estimate error $e(t)$ to zero. The delay τ_{2x} represents the additional time lag introduced into the feedback loop by the observer's processing and communication.

$$\begin{cases} \dot{\hat{x}}(t) = A \hat{x}(t) + B u(t - \tau_{1x}) + L_x [y(t - \tau_{2x}) - \hat{y}(t - \tau_{2x})] \\ \hat{y}(t) = C \hat{x}(t) \end{cases} \quad (14)$$

The observer gains $L_x = [l_{x1} \quad l_{x2}]^T$ (and similarly $L_y = [l_{y1} \quad l_{y2}]^T$) represent the weighting factors that determine how strongly the observer corrects its state estimate based on the discrepancy between the measured output $y(t)$ and the estimated output $\hat{y}(t)$. Specifically, l_{x1} influences the correction of the estimated position error, while l_{x2} influences the correction of the estimated velocity error (as can be inferred from the structure of the observer dynamics in (14)). In a practical sense, larger values for these gains generally lead to faster convergence of the estimated states to the true states, meaning the observer reacts more quickly to errors. However, excessively large gains can also amplify measurement noise, leading to a less smooth state estimate and potentially to oscillatory behavior or even instability in the closed-loop system, especially in the presence of delays as analyzed.

The selection of l_{x1} and l_{x2} (and l_{y1}, l_{y2}) thus involves a trade-off between the speed of state estimation and sensitivity to noise and unmodeled dynamics. The stability regions, like those shown in figure 3 and figure 4, define the permissible combinations of these gains that ensure the observer error itself remains stable, providing a crucial guideline for their practical selection to achieve robust and accurate state estimation.

Given the state feedback controller defined by:

$$u(t) = -K_x \hat{x}(t) \quad (15)$$

We determine the formula that governs the progression of the error:

$$se(s) = (A - L_x C e^{-\tau_{2x}s}) e(s) \quad (16)$$

The characteristic equation is:

$$H(s, l_{x1}, l_{x2}, \tau_{2x}) = \det(L_x C e^{-\tau_{2x}s} + sI_2 - A) \quad (17)$$

3.2. Routh-Hurwitz Stability Analysis

This analysis allows for the identification of elements that ensure stability in relation to the observer. To achieve this, we first examine a scenario where the lag τ_{2x} is equal to zero. In this case, substituting $\tau_{2x} = 0$ (thus $e^{-\tau_{2x}s} = 1$) into the characteristic equation (17), and given $A = \begin{bmatrix} 0 & 1 \\ 0 & 0 \end{bmatrix}$, $C = [1 \quad 0]$, and $L_x = [l_{x1} \quad l_{x2}]^T$, we have:

$$H(s) = \det(L_x C e^{-\tau_{2x}s} + sI_2 - A) = \det\left(\begin{bmatrix} l_{x1} \\ l_{x2} \end{bmatrix} [1 \quad 0] + \begin{bmatrix} s & 0 \\ 0 & s \end{bmatrix} - \begin{bmatrix} 0 & 1 \\ 0 & 0 \end{bmatrix}\right)$$

Thus, (17) can be expressed as:

$$H(s) = s^2 + s l_{x1} + l_{x2} \quad (18)$$

For this second-order polynomial, the Routh-Hurwitz stability criterion requires all coefficients to be positive for a stable system (as the first coefficient, $a_0=1$, is already positive). Therefore, for stability, we must have:

$$l_{x1} > 0, \quad l_{x2} > 0 \quad (19)$$

3.3. The System Stability: Geometric Approach

In this section, we will conduct a comprehensive analysis of the overall stability of the system with a non-zero delay τ_{2x} . To achieve this, we employ a geometric approach. The core idea of this method is to find the boundaries of stability in the plane of the observer parameters (l_{x1}, l_{x2}) by determining the conditions under which the characteristic equation (17) has purely imaginary roots, i.e., $s = j\omega$ where ω is a real frequency. Such roots signify that the system is on the verge of instability, at the boundary between stable and unstable regions. Therefore, substituting $s = j\omega$ into (17) gives:

$$\forall \omega \in \mathcal{R}^+, \quad \exists \tau_{2x}^* \in \mathcal{R}^+, \quad H(j\omega, l_{x1}, l_{x2}, \tau_{2x}^*) = 0 \quad (20)$$

In order for (20) to be satisfied, both its real and imaginary parts must independently be equal to zero. This separation leads to two real equations:

$$\begin{cases} -\omega^2 + \omega l_{x1} \sin(\omega \tau_{2x}^*) + l_{x2} \cos(\omega \tau_{2x}^*) = 0 \\ \omega l_{x1} \cos(\omega \tau_{2x}^*) - l_{x2} \sin(\omega \tau_{2x}^*) = 0 \end{cases}$$

i.e. :

$$l_{x1} = \omega \sin(\omega \tau_{2x}^*) \quad (21)$$

$$l_{x2} = \omega^2 \cos(\omega \tau_{2x}^*) \quad (22)$$

Equations (21) and (22) define a parametric curve in the (l_{x1}, l_{x2}) plane, with ω (where $\omega > 0$) serving as the parameter. For a fixed delay τ_{2x} , as ω varies, this curve traces the stability boundary. Points (l_{x1}, l_{x2}) on one side of this boundary will correspond to a stable observer, while points on the other side will correspond to an unstable one. The stability region itself, shown for example in [figure 3](#), is the graphical representation of the set of (l_{x1}, l_{x2}) pairs satisfying the stability conditions derived from this approach.

Next, to determine the direction of transition across this stability boundary (i.e., whether the system moves from unstable to stable or vice-versa as a root crosses the imaginary axis), we analyze the sign of the expression $R_2 I_1 - R_1 I_2$. This analysis is based on established stability-crossing theorems [11], which examine how roots of the characteristic equation traverse the imaginary axis. Here, R_i and I_i are the real and imaginary parts derived from the partial derivatives of the characteristic function with respect to the parameters l_{x1} and l_{x2} , evaluated at $s = j\omega$, as defined in (23) and (24) respectively. The sign of the expression $R_2 I_1 - R_1 I_2$ indicates the direction in which the roots cross the imaginary axis.

$$R_1 + jI_1 = -\frac{1}{s} \frac{\partial H(s, l_{x1}, l_{x2}, \tau_{2x}^*)}{\partial l_{x2}} \Big|_{s=j\omega} \quad (23)$$

$$R_2 + jI_2 = -\frac{1}{s} \frac{\partial H(s, l_{x1}, l_{x2}, \tau_{2x}^*)}{\partial l_{x1}} \Big|_{s=j\omega} \quad (24)$$

After obtaining the expressions of R_i and I_i , we have:

$$R_2 I_1 - R_1 I_2 = -\frac{1}{\omega} < 0 \quad (25)$$

This indicates that when ω increases in the positive direction, a solution of (20) passes through the imaginary axis moving to the left. Therefore, by utilizing equations (19), (21), (22), and (25), and considering that τ_{2x}^* is equal to 0.4 seconds, we have determined the stability region, as illustrated in [figure 3](#). Each point (l_{x1}^*, l_{x2}^*) within the stability zone corresponds to a specific observer gain L_x^* where the characteristic equation, defined by $H(l_{x1}^*, l_{x2}^*, \tau_{2x}) = 0$, is stable for all delays less than the critical delay τ_{2x}^* .

3.4. Critical Delay

To determine the critical delay τ_{2x}^* , an examination of the stability threshold is conducted, which occurs when (17) has a purely imaginary root. Thus, we have:

$$\cos(\omega \tau_{2x}^*) - j \sin(\omega \tau_{2x}^*) = \frac{\omega^2}{j\omega l_{x1}^* + l_{x2}^*}$$

Therefore, the critical delay is:

$$\tau_{2x}^* = \frac{1}{\omega} \text{Arccos} \left[\frac{l_{x2}^* \omega^2}{(l_{x2}^*)^2 + (\omega l_{x1}^*)^2} \right] \quad (26)$$

3.5. Observer on the y-axis

Following the approach outlined earlier, we determine the stability region along the y-direction. Figure 4 illustrates this region for $\tau_{2y}^* = 1$ s. The critical delay τ_{2y}^* is defined as follows:

$$\tau_{2y}^* = \frac{1}{\omega} \text{Arccos} \left[\frac{l_{y2}^* \omega^2}{(l_{y2}^*)^2 + (\omega l_{y1}^*)^2} \right] \quad (27)$$

For a specific set of observer gains (l_{x1}, l_{x2}) selected from the stable region (figure 3), Equation (26) is used to analytically compute the maximum delay τ_{2x} for which the observer remains stable. Similarly, Equation (27) is used for the y-axis with gains (l_{y1}, l_{y2}) . The frequency ω used in these formulas corresponds to the critical crossing frequency associated with the chosen gains. This frequency is determined by first considering (20). By separating the real and imaginary parts of this complex equation, the critical delay τ_{2x}^* can be eliminated, allowing the determination of the critical crossing frequency ω that satisfies the boundary condition for stability, given l_{x1} and l_{x2} . The detailed derivation methodology is presented in [1]. Once this critical frequency ω is found, it is then used in Equations (26) and (27) to compute the corresponding critical delays τ_{2x}^* and τ_{2y}^* .

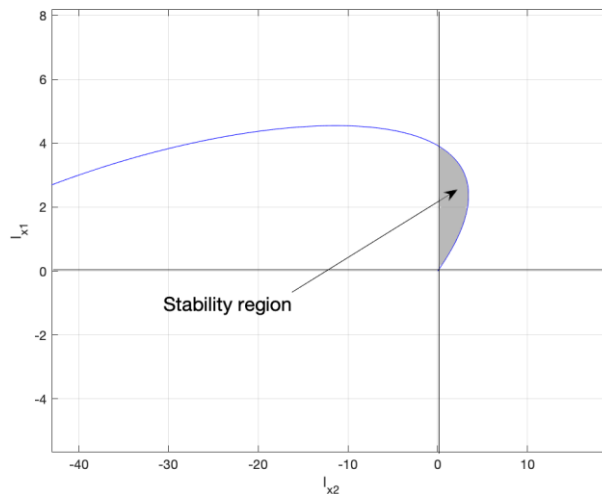


Figure 3. Stability region in the (l_{x2}, l_{x1}) plane for the observer gains with delay $\tau_{2x}^* = 0.4$ s. The shaded area represents combinations of l_{x1} and l_{x2} for which the observer is stable

4. Results And Discussion

To verify the obtained results, we examine the ball-and-plate system described in [1]. Our objective is to regulate the ball's position on the plate while ensuring minimal estimation errors. To confirm this, we will test multiple observer gain values L_x and L_y . These vectors correspond to the areas illustrated in figure 3 and figure 4. The critical delays are determined using (26) and (27). The obtained results are shown in table 1 and table 2.

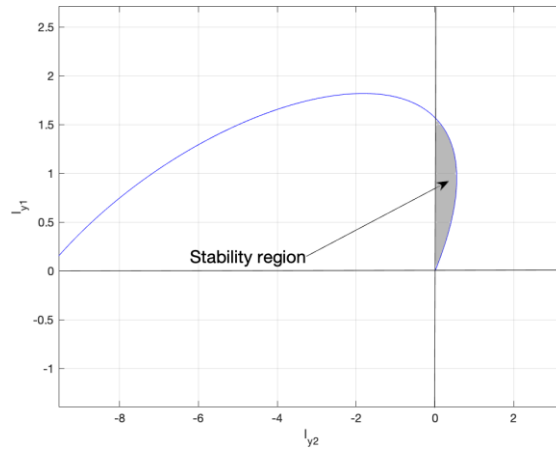


Figure 4. Stability region in the (l_{y2}, l_{y1}) plane for the observer gains with delay $\tau_{2y}^* = 1s$. The shaded area represents combinations of l_{y1} and l_{y2} for which the observer is stable.

By using the observer gains from table 1 and table 2, selected from within the stable regions depicted in figure 3 and figure 4, we have determined the trajectory of the ball position, as shown in figure 5 and figure 6. Furthermore, the temporal evolution of the observer errors $e_1(t)$ and $e_2(t)$ are presented in figure 7, figure 8, figure 9, and figure 10.

Table 1. Chosen gains along the x-axis

(l_{x1}^*, l_{x2}^*)	L_x^*	τ_{2x}^*
(3.68, 0.76)	$L_1 = [3.68 \ 0.76]^T$	0.4109
(2.67, 2.79)	$L_2 = [2.67 \ 2.79]^T$	0.4284
(1.58, 1.35)	$L_3 = [1.58 \ 1.35]^T$	0.6364

Table 2. Chosen gains along the y-axis

(l_{y1}^*, l_{y2}^*)	L_y^*	τ_{2y}^*
(1.66, 0.1)	$L_4 = [1.66 \ 0.1]^T$	0.9238
(1.15, 0.39)	$L_5 = [1.15 \ 0.39]^T$	1.0827
(0.58, 0.27)	$L_6 = [0.58 \ 0.27]^T$	1.4084

For the x-axis motion, as detailed in figure 5, gain L_3 (1.58, 1.35) appears to offer the fastest convergence to the origin with minimal oscillations after the initial transient, suggesting a well-damped response. Gain L_1 (3.68, 0.76), while also stable, exhibits a slightly slower response. Meanwhile, gain L_2 (2.67, 2.79) shows a reasonable convergence speed, possibly with a slightly different transient behavior compared to L_3 .

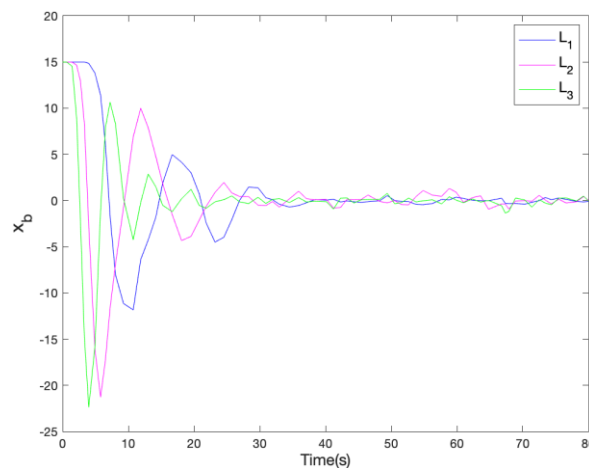


Figure 5. Temporal evolution of the ball's x-coordinate (x_b) for different observer gains L_1 , L_2 , and L_3 .

Turning to the y-axis motion illustrated in [figure 6](#), gain L_5 (1.15, 0.39) seems to provide a good balance, leading to a relatively fast response with controlled overshoot.

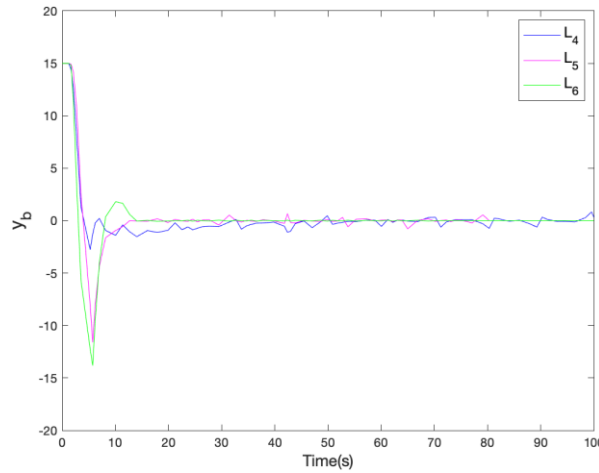


Figure 6. Temporal evolution of the ball's x-coordinate (y_b) for different observer gains L_4 , L_5 , and L_6 .

Gain L_4 (1.66, 0.1) might result in a quicker initial response but potentially with more pronounced overshoot. Conversely, L_6 (0.58, 0.27), having the largest critical delay τ_{2y}^* , might offer a smoother but potentially slower response. These qualitative observations highlight that the choice of observer gains within the stable region significantly impacts the transient response characteristics of the system.

The simulation results, presented in [figure 5](#), [figure 6](#), [figure 7](#), [figure 8](#), [figure 9](#) and [figure 10](#), illustrate the performance of the designed controller and observer. As observed from the ball trajectories in [figure 5](#) and [figure 6](#), the dynamic behavior of the system is indeed sensitive to the specific choice of observer gains L_x and L_y , even when these are selected from within the derived stable regions ([figure 3](#) and [figure 4](#)). For instance, along the x-axis ([figure 5](#)), gain L_3 appears to offer the most effective speed of convergence. Similarly, for the y-axis ([figure 6](#)), L_5 demonstrates comparatively rapid and well-damped performance. This highlights that different gains within the stable zone can be chosen to prioritize certain performance aspects, such as minimizing initial overshoot (potentially with a gain like L_4 for the y-axis) or ensuring faster settling, illustrating the inherent trade-offs in control design. While this qualitative analysis provides valuable insights, a more rigorous selection process would benefit from quantitative performance metrics.

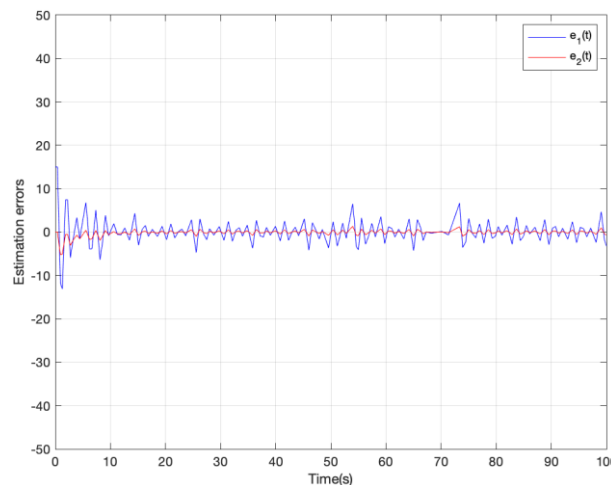


Figure 7. Time evolution of the estimation errors $e_1(t)$ (position error) and $e_2(t)$ (velocity error) for observer gain L_1 .

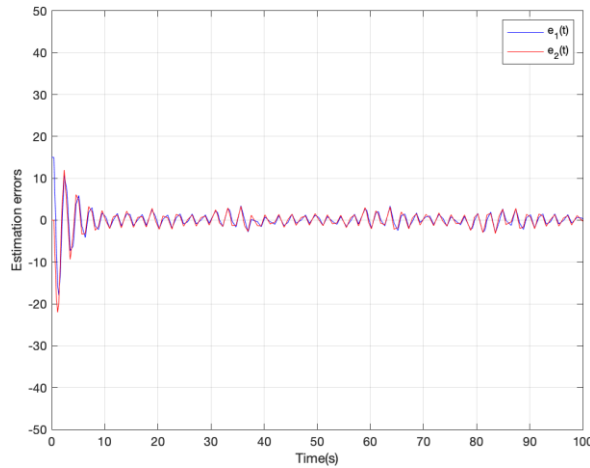


Figure 8. Time evolution of the estimation errors $e_1(t)$ (position error) and $e_2(t)$ (velocity error) for observer gain L_2 . Furthermore, [figure 7](#), [figure 8](#), [figure 9](#) and [figure 10](#) confirm the convergence of the estimation errors for representative observer gains, indicating that the Luenberger observer successfully tracks the system states. For the designated gains, such as L_3 and L_6 which are designed to operate up to their respective critical delays (τ_{2x}^* and τ_{2y}^* as per [table 1](#) and [table 2](#)), the simulations demonstrate that the closed-loop system maintains stability and achieves the control objective of steering the ball to the origin (0,0).

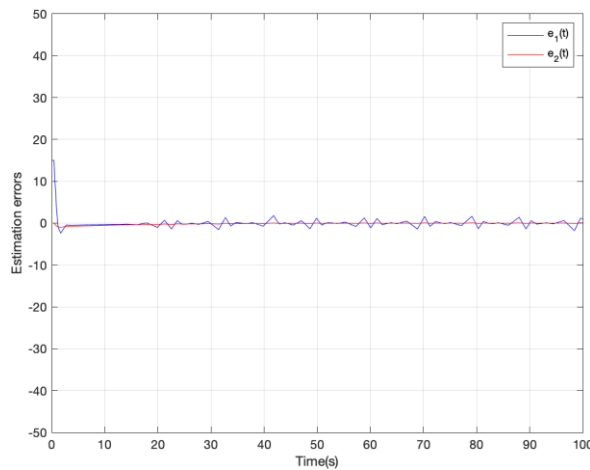


Figure 9. Time evolution of the estimation errors $e_1(t)$ (position error) and $e_2(t)$ (velocity error) for observer gain L_4 .

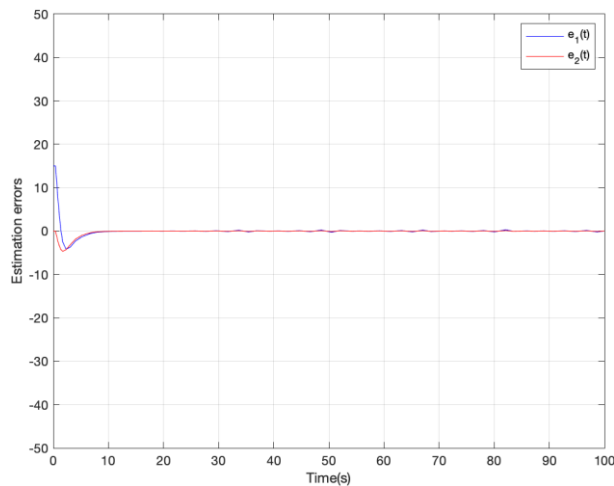


Figure 10. Time evolution of the estimation errors $e_1(t)$ (position error) and $e_2(t)$ (velocity error) for observer gain L_5 .

It is important to contextualize these findings: the presented simulation results were obtained under ideal conditions, without the inclusion of external disturbances or significant measurement noise. This study has primarily focused on the stability analysis methodology in the presence of known feedback and observer delays. Consequently, while the controller and observer demonstrate effective performance under these conditions within the calculated critical delay ranges, their robustness to unmodeled dynamics, external disturbances, or measurement noise has not been explicitly tested. A rigorous proof of convergence under more general conditions, or a thorough analysis of robustness to such practical imperfections, would constitute important areas for further investigation and represent valuable extensions to this work.

5. Conclusion

This study explores the regulation of the ball and plate system through a geometric approach. The designed controller integrates a state feedback mechanism with a Luenberger observer. This allows for state estimation, enhancing the system's control efficiency. The outcomes of the simulations validate the effectiveness of our method. However, we face challenges in selecting the optimal gains L_x and L_y based purely on the stability regions derived from the geometric approach. As observed qualitatively in Section 4, different gains within the stable region yield varied transient responses. Therefore, we recommend that future research focus on developing an algorithm or a systematic methodology for selecting optimal observer gains. This could involve defining a multi-objective cost function that includes standard performance metrics such as rise time, settling time, percentage overshoot, and integral error criteria (e.g., IAE, ISE), as well as a measure of robustness to delay variations or noise sensitivity. Optimization techniques such as Particle Swarm Optimization (PSO), Genetic Algorithms (GA), or gradient-based methods could then be employed to search for gains within the pre-identified stable regions that minimize this cost function. This would allow for more precise and automated tuning of the observer based on specific desired performance trade-offs. Additionally, further research could focus on rigorously analyzing the system's robustness to external disturbances and measurement noise, potentially incorporating adaptive or robust control techniques to enhance performance under real-world conditions.

6. Declarations

6.1. Author Contributions

Conceptualization: K.L. and S.T.; Methodology: S.T.; Software: K.L.; Validation: K.L. and S.T.; Formal Analysis: K.L. and S.T.; Investigation: K.L.; Resources: S.T.; Data Curation: S.T.; Writing Original Draft Preparation: K.L. and S.T.; Writing Review and Editing: K.L. and S.T.; Visualization: K.L.; All authors have read and agreed to the published version of the manuscript.

6.2. Data Availability Statement

The data presented in this study are available on request from the corresponding author.

6.3. Funding

The authors received no financial support for the research, authorship, and/or publication of this article.

6.4. Institutional Review Board Statement

Not applicable.

6.5. Informed Consent Statement

Not applicable.

6.6. Declaration of Competing Interest

The authors declare that they have no known competing financial interests or personal relationships that could have appeared to influence the work reported in this paper.

References

- [1] K. Lefrouni and S. Taibi, "State-Feedback Control of Ball-Plate System: Geometric Approach," *International Journal of Advanced Computer Science and Applications*, vol. 15, no. 3, pp. 968–974, 2024, doi: 10.14569/IJACSA.2024.0150396.

- [2] S. Palagummi and F. G. Yuan, "Magnetic levitation and its application for low frequency vibration energy harvesting," in *Structural Health Monitoring (SHM) in Aerospace Structures*, F. G. Yuan, E. L. Flesch, and S. S. K. Tadigadapa, Eds. Cambridge, UK: Woodhead Publishing, 2016, ch. 8, pp. 213–251, doi: 10.1016/B978-0-08-100148-6.00008-1.
- [3] S. Zaare and M. R. Soltanpour, "The position control of the ball and beam system using state-disturbance observe-based adaptive fuzzy sliding mode control in presence of matched and mismatched uncertainties," *Mechanical Systems and Signal Processing*, vol. 150, no. 2, pp. 1-14, 2021, doi: 10.1016/j.ymsp.2020.107243
- [4] H. Alpaslan and L. Gören-Sümer, "Stabilizing of Ball and Plate System Using an Approximate Model," *IFAC-PapersOnLine*, vol. 50, no. 1, pp. 9601–9606, Jul. 2017, doi: 10.1016/j.ifacol.2017.08.1688
- [5] D. Udekwe, O. Ajayi, O. Ubadike, K. Ter, and E. Okafor, "Comparing actor-critic deep reinforcement learning controllers for enhanced performance on a ball-and-plate system," *Expert Systems with Applications*, vol. 245, no. 6, pp. 1-11, 2024, doi: 10.1016/j.eswa.2023.123055.
- [6] L. Zhou, H. Brunskill, and R. Lewis, "Experimental investigation on ball plate contact using ultrasonic reflectometry: From static to dynamic," *Ultrasonics*, vol. 124, no. 7, pp. 1-9, 2022, doi: 10.1016/j.ultras.2022.106733.
- [7] Y. Huawen and X. Honglei, "Global stabilization for ball-and-beam systems via state and partial state feedback," *Journal of Industrial and Management Optimization*, vol. 12, no. 1, pp. 17–29, Jan. 2016, doi: 10.3934/jimo.2016.12.17.
- [8] Z. Chen, F. Gao, Q. Sun, Y. Tian, J. Liu, and Y. Zhao, "Ball-on-plate motion planning for six-parallel-legged robots walking on irregular terrains using pure haptic information," *Mechanism and Machine Theory*, vol. 141, no. 11, pp. 136–150, 2019, doi: 10.1016/j.mechmachtheory.2019.07.009
- [9] M. K. Choudhary and G. N. Kumar, "ESO Based LQR Controller for Ball and Beam System," *IFAC-PapersOnLine*, vol. 49, no. 1, pp. 607–610, 2016, doi: 10.1016/j.ifacol.2016.03.122.
- [10] H. A. Yaseen, "A comparative study of stabilizing control of a planer electromagnetic levitation using PID and LQR controllers," *Results in Physics*, vol. 7, no. 1, pp. 4379–4387, 2017, doi: 10.1016/j.rinp.2017.11.007.
- [11] Y. Wen and F. Ortiz, "Stability analysis of PD regulation for ball and beam system," in Proc. 2005 IEEE Conf. Control Appl. (CCA), Portland, OR, USA, 2005, pp. 517–522, doi: 10.1109/CCA.2005.1507178.
- [12] B. Manashita, R. Prasanta, and R. Binoy, "Enhanced Performance in Trajectory Tracking of a Ball and Plate System using Fractional Order Controller," *IETE Journal of Research*, vol. 64, no. 2, pp. 232–241, Mar.–Apr. 2018, doi: 10.1080/03772063.2017.1343157.
- [13] S. Oh, H. Jang, and W. Pedrycz, "Optimized fuzzy PD cascade controller: A comparative analysis and design," *Simulation Modelling Practice and Theory*, vol. 19, no. 1, pp. 181–195, Jan. 2011, doi: 10.1016/j.simpat.2010.06.004
- [14] J. H. Park and Y. J. Lee, "Robust visual servoing for motion control of the ball on a plate," *Mechatronics*, vol. 13, no. 7, pp. 723–738, Sep. 2003, doi: 10.1016/S0957-4158(02)00039-9
- [15] H. Bang and Y. S. Lee, "Implementation of a Ball and Plate Control System Using Sliding Mode Control," *IEEE Access*, vol. 6, no. 5, pp. 32401–32408, 2018, doi: 10.1109/ACCESS.2018.2838544
- [16] T. Basant, K. Narendra, and S. Mini, "Augmentation in Performance of Real-Time Balancing and Position Tracking Control for 2-DOF Ball Balancer System Using Intelligent Controllers," *Wireless Personal Communications*, vol. 138, no. 3, pp. 2227–2257, Sep. 2024, doi: 10.1007/s11277-024-11591-5
- [17] J. Ma, C. L. Wang, Y. Zhou, and R. D. Wang, "Optimized design of a linear Fresnel collector with a compound parabolic secondary reflector," *Renewable Energy*, vol. 171, no. 6, pp. 141–148, 2021, doi: 10.1016/j.renene.2021.02.100.
- [18] E. Mitterand, A. Omer, S. Iman, and S. Raafat, "Metaheuristic Approaches to Tune PID Controller for Ball on Plate System," *Advances in Computational Intelligence and Computer Engineering*, vol. 944, no. 5, pp. 121–135, 2024, doi: 10.1007/978-3-031-52965-8_10
- [19] C. C. Cheng and C. H. Tsai, "Visual servo control for balancing a Ball-Plate system," *International Journal of Mechanical Engineering and Robotics Research*, vol. 5, no. 1, pp. 28–32, Jan. 2016, doi: 10.18178/ijmerr.5.1.28-32.
- [20] M. Hamdoun, A. Errahali, K. Hissi, N. E. L. Mouchtarii, and S. K. Ameer, "Functional observer-based feedback controller for ball balancing table," *SN Applied Sciences*, vol. 3, no. 6, pp. 1-12, 2021, doi: 10.1007/s42452-021-04590-9
- [21] A. Wang, X. Li, S. He, X. Cao, Y. Jing, and M. Chen, "Command-Filtering-Based Adaptive Finite-Time Tracking Control for Ball and Plate System," *IFAC-PapersOnLine*, vol. 53, no. 2, pp. 6165–6170, 2020, doi: 10.1016/j.ifacol.2020.12.1700.
- [22] K. Lefrouni, Y. Moubachir, and S. Taibi, "Control of Ball-Plate System with Observer-Based State-Feedback and Geometric Considerations," *International Journal of Difference Equations*, vol. 16, no. 1, pp. 35–46, 2021, doi : 10.4067/S0718-33052020000100006.

- [23] D. G. Luenberger, "An Introduction to Observers," *IEEE Transactions on Automatic Control*, vol. AC-16, no. 6, pp. 596–602, Dec. 1971, doi: 10.1109/TAC.1971.1099826
- [24] E. Frazzoli and M. Dahleh, *Dynamic Systems and Control*. MIT OpenCourseWare, Massachusetts Institute of Technology, Spring 2011.